Supplementary Information for

Surface-Percolated GNP Coatings on 3D-Printed PLA Lattices for Tunable EMI Shielding and Flame-Retardant Multifunctionality

Najmeh Taala[1], Mohammad Aberoumand[1], Erick Gabriel Ribeiro dos Anjos[1,2], Uttandaraman Sundararaj[1*]

1. Department of Chemical and Petroleum Engineering, University of Calgary, Calgary, AB T2L1Y6, Canada
2. Department of Science and Technology, Federal University of São Paulo, São José dos Campos, São Paulo, Brazil

Peeling test

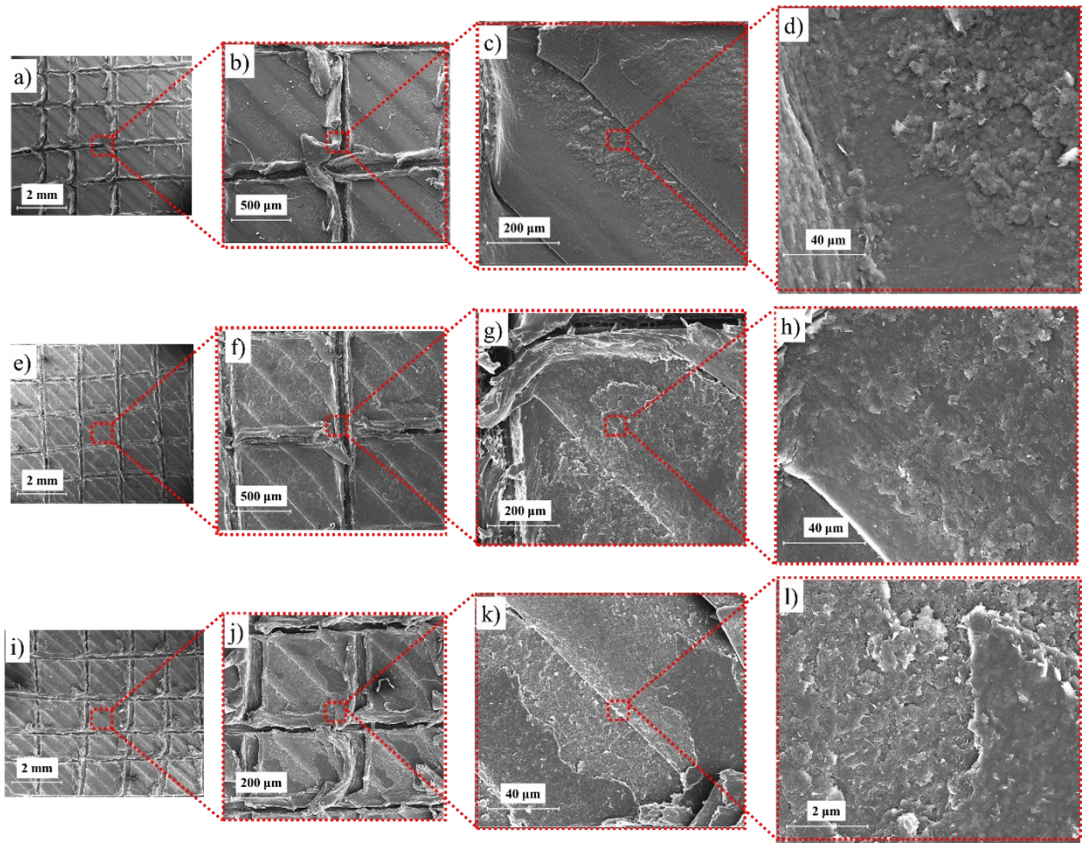

Figure S1. FESEM micrographs (secondary electron mode) of PLA scaffolds after peel testing for adhesion control experiments conducted with 3 GNP dip-coating cycles: (a–d) untreated PLA, (e–h) NaOH-etched PLA, and (i–l) PEI-modified PLA. Increasing magnifications illustrate coating retention after mechanical peeling.

To decouple the effects of surface roughening and surface functionalization on coating adhesion, samples were prepared using identical dip-coating conditions (3 coating cycles) and subjected to

peel testing. FESEM examination of the post-peel fracture surfaces reveals distinct differences in coating adhesion depending on surface pretreatment.

Untreated PLA exhibits negligible residual GNP coverage after peeling, indicating weak interfacial adhesion. NaOH-etched PLA demonstrates improved coating adhesion relative to untreated PLA, suggesting that surface roughening enhanced mechanical interlocking. PEI-modified PLA showed further improvement in residual GNP presence after peeling, consistent with additional interfacial interactions introduced by surface functionalization.

However, compared to the combined NaOH + PEI treatment reported in the main manuscript, these single-treatment controls exhibit visibly weaker coating adhesion. The combined treatment provides the highest coating adhesion among the tested conditions, with substantially reduced delamination after peel testing. These comparative results support the interpretation that both surface texturing and interfacial modification contribute to enhanced GNP coating adhesion.

EMI shielding:

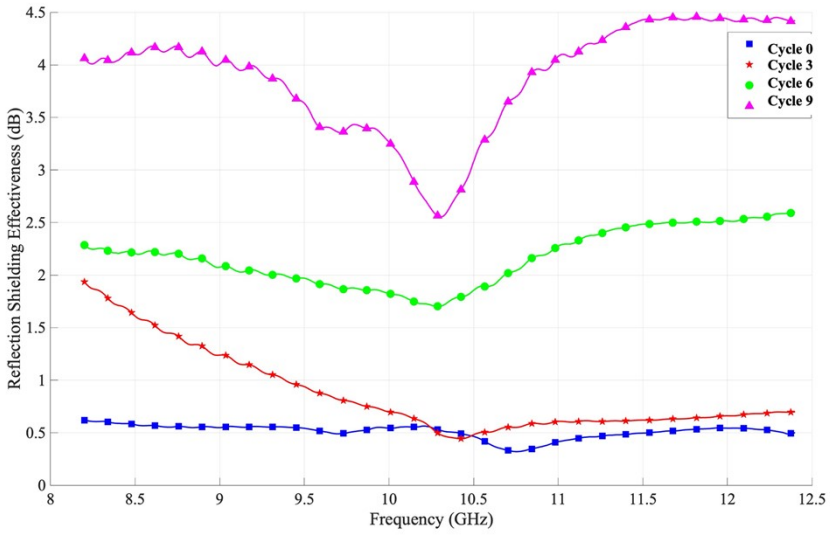

Figure S2. Reflection shielding effectiveness versus frequency for 3D-printed PLA samples coated for 0, 3, 6, and 9 cycles.

Figure S2 shows the reflection component of the shielding effectiveness (SER) for PLA lattice samples subjected to 0, 3, 6, and 9 dip-coating cycles. The results demonstrate a gradual and consistent increase in SE_R as the number of coating cycles increases, confirming that each additional graphene nanoplatelet (GNP) deposition enhances the material's reflective shielding

capability. This improvement is attributed to the progressive buildup of conductive GNP layers, which increase surface conductivity, reduce interfacial defects, and promote a more uniform electromagnetic (EM) barrier.

Across all coating cycles, the SE_R curves display a characteristic dip near 10–10.5 GHz, followed by recovery at higher frequencies. This dip may be associated with resonance-like behavior of the porous architecture, where the interplay between coating conductivity, lattice geometry, and dielectric properties can produce localized impedance-matching conditions [1]. Under this condition, the structure allows more EM energy to enter and dissipate within the coating–pore network, rather than being fully reflected. Such behavior is desirable for absorption-dominant EMI shielding systems, in which both surface reflection and internal loss contribute to overall shielding performance.

The position and depth of the SE_R trough evolved consistently with increasing coating cycles, suggesting that resonance-like behavior may be associated with Fabry–Pérot-type interference, cavity-mediated effects within the porous lattice, and interfacial polarization at GNP–PLA boundaries [2–4]. This trend suggests a gradual shift from a primarily reflection-dominated response toward a more balanced reflection–absorption behavior as the number of coating cycles increases.

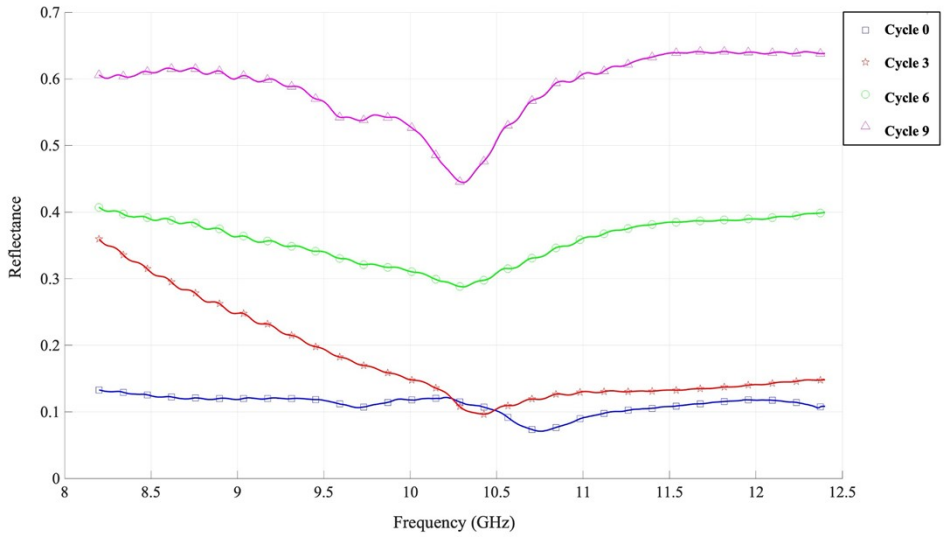

Figure S3. Reflectance versus frequency for 3D-printed PLA samples coated for 0, 3, 6, and 9 cycles.

Figures S3 and S4 illustrate the reflectance (R) and absorbance (A) profiles of the porous PLA structures across the X-band as a function of coating cycles. As shown, distinct dips in reflectance accompanied by corresponding peaks in absorbance consistently appear in the 10–11 GHz region. With additional dip-coating cycles, these spectral features gradually shift toward lower frequencies and increase in magnitude, indicating a strong dependence on the evolving electrical properties of the GNP layer.

Importantly, the presence of measurable absorbance peaks even in the uncoated sample (0 cycles) confirms that the resonant behavior originates not only from the conductive coating but also from the intrinsic porosity and geometry of the lattice, supporting the trends observed previously in Figure 14. The porous architecture may therefore act as a structural resonator capable of coupling with incident electromagnetic (EM) waves.

These frequency-localized features may be influenced by geometry-driven absorption mechanisms, including cavity resonance and Fabry–Pérot interference, where EM waves are confined between partially reflective boundaries which can give rise to standing-wave–like field distributions [5–7]. The resonance frequency is strongly governed by pore size, lattice spacing, and internal cavity dimensions, all of which determine the effective path length for constructive interference.

An additional contributing factor may be frequency-dependent polarization and relaxation processes within the conductive GNP network. When the incident EM wave frequency aligns with the characteristic oscillation modes of the conductive GNP layer, additional absorption may occur due to enhanced polarization and relaxation losses.

The progressive red-shift (shift toward lower frequency) observed with increasing coating cycles may reflect the combined influence of the thickening conductive layer and geometry-induced resonance-like behavior in the porous structure. As the coating becomes thicker, smoother, and more conductive, the influence of the GNP-dominated resonance grows, gradually increasing the contribution of coating-dominated effects relative to purely geometric responses [8,9].

Finally, the increasing height of the absorbance peaks may be associated with enhanced frequency-selective attenuation, supported by higher surface conductivity, reduced interfacial resistance, and

more uniform EM energy trapping as the GNP layer becomes more continuous with increasing cycles.

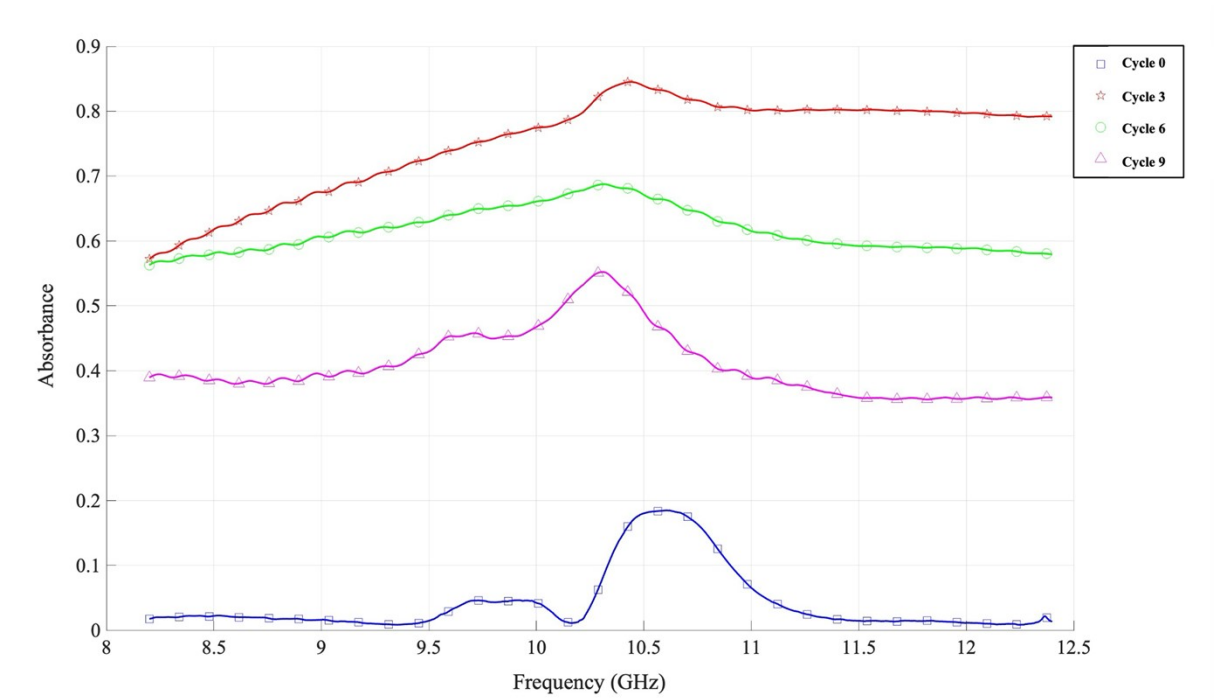

Figure S4. Absorbance versus frequency for 3D-printed PLA samples coated for 0, 3, 6, and 9 cycles.

Flame retardancy:

Figure S5 presents FESEM images of the char residues formed after combustion for samples coated for 3, 6, and 9 cycles. These images provide detailed insight into how the char structure evolves as the GNP layer becomes thicker and more continuous. The layered graphene coating can act as an oxygen-diffusion barrier and a heat-dissipation pathway due to the intrinsic thermal conductivity of graphene nanoplatelets [10]. This combined barrier and thermal redistribution effect likely contributes to delayed ignition, stabilizes the polymer during thermal degradation, and suppresses the generation of volatile, flammable pyrolysis products. Correspondingly, the char becomes progressively smoother and less porous as coating cycles increase, indicating the formation of a more cohesive protective layer.

The FESEM observations in Figure S5 show the development of a dense, crack-resistant char structure at higher coating cycles. This behavior is consistent with the formation of a denser barrier layer, which can improve thermal shielding and structural integrity during combustion. In addition, a combined effect between the conductive GNP coating and the underlying porous diamond-like lattice is observed. The high surface-area-to-volume ratio of the lattice may facilitate heat redistribution and reduce localized thermal gradients that typically lead to catastrophic structural collapse [11].

Moreover, the interconnected porous network may provide pathways for the gradual release of gaseous pyrolysis products, which can reduce local pressure buildup and help preserve the char structure. Instead of rupturing or collapsing abruptly, the char layer appears to expand and stabilize, allowing the structure to remain intact under extended thermal exposure. This controlled venting mechanism may contribute to char cohesion and reduced internal pressure buildup during decomposition. These findings are consistent with the preserved structural morphology of the burnt samples shown in Figures 16(c), 16(e), and 16(g), confirming the combined protective roles of the GNP coating and the 3D-printed lattice geometry in enhancing flame retardancy [12].

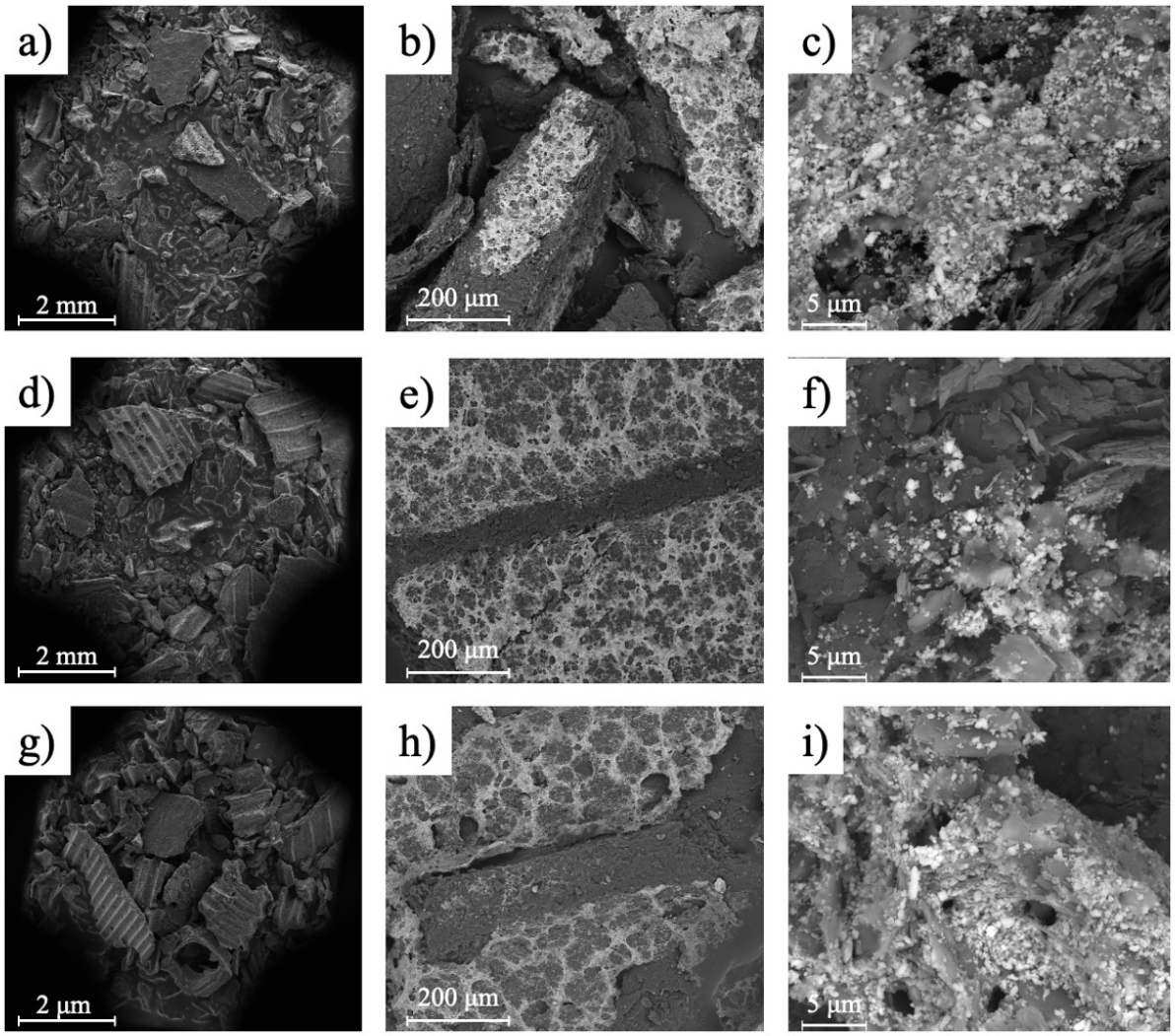

Figure S5. FESEM images of ashes of porous 3D printed PLA samples coated for (a-c) 3, (d-f) 6, and(g-i) 9 times at various magnifications acquired in secondary-electron mode (first column) and back-scattered electron mode (second and third columns), respectively.

References

[1] J. Wang, F. Wu, Y. Cui, A. Zhang, Q. Zhang, B. Zhang, Efficient synthesis of N-doped porous carbon nanoribbon composites with selective microwave absorption performance in common wavebands, Carbon 175 (2021) 164–175. https://doi.org/10.1016/J.CARBON.2021.01.005.

[2] H. Li, Z. Yin, C. Zhang, Y. Zhang, R. Deng, H. Dong, S. Wang, L. Zhang, Fabry–Perot resonance-suppressed double-layer metal mesh window for electromagnetic interference shielding, Optics Letters, Vol. 47, Issue 20, Pp. 5393-5396 47 (2022) 5393–5396. https://doi.org/10.1364/OL.474330.

[3] J.H. Park, J. Park, F. Tang, Y.G. Song, Y.G. Jeong, Electromagnetic Interference Shielding and Joule Heating Properties of Flexible, Lightweight, and Hydrophobic MXene/Nickel-Coated Polyester Fabrics Manufactured by Dip-Dry Coating and Electroless Plating, ACS Appl Mater Interfaces 16 (2024) 38490–38500. https://doi.org/10.1021/ACSAMI.4C06735/ASSET/IMAGES/LARGE/AM4C06735_0009.JPEG.

[4] Y. Du, Y. Liu, A. Wang, J. Kong, Research progress and future perspectives on electromagnetic wave absorption of fibrous materials, IScience 26 (2023). https://doi.org/10.1016/J.ISCI.2023.107873.

[5] B. Ribeiro, N.A.S. Gomes, M. Baldan, M.C. Rezende, Designing Sandwich Architecture Towards Glass Fiber/Epoxy Reinforced Multi-walled Carbon Nanotube Buckypaper Composites for Electromagnetic Interference Shielding, Electronic Materials Letters 19 (2023) 184–191. https://doi.org/10.1007/S13391-022-00382-4/TABLES/2.

[6] W.L. Song, L.Z. Fan, M.S. Cao, M.M. Lu, C.Y. Wang, J. Wang, T.T. Chen, Y. Li, Z.L. Hou, J. Liu, Y.P. Sun, Facile fabrication of ultrathin graphene papers for effective electromagnetic shielding, J Mater Chem C Mater 2 (2014) 5057–5064. https://doi.org/10.1039/C4TC00517A.

[7] G. Alagappan, F.J. García-Vidal, C.E. Png, Fabry-Perot Resonances in Bilayer Metasurfaces, Phys Rev Lett 133 (2024) 226901. https://doi.org/10.1103/PHYSREVLETT.133.226901/SUPPLEMENTAL_MATERIAL_REVISED.PDF.

[8] U. Hwang, J. Lee, S. Kim, X. Yang, S. Kim, J. Suhr, J. Do Nam, Structural Design of Hybrid Fillers in a Polymer Matrix for Advanced Electromagnetic Interference Shielding, Small Struct 6 (2025) 2400404. https://doi.org/10.1002/SSTR.202400404.

[9] Y. Gao, Z. Wang, Microwave absorption and electromagnetic interference shielding properties of Li-Zn ferrite-carbon nanotubes composite, J Magn Magn Mater 528 (2021) 167808. https://doi.org/10.1016/J.JMMM.2021.167808.

[10] R.S. Chen, N.A. Mohd Amran, S. Ahmad, Reinforcement effect of nanocomposites with single/hybrid graphene nanoplatelets and magnesium hydroxide: Thermal stability, flame retardancy and mechanical performance, J Therm Anal Calorim 137 (2019) 79–92. https://doi.org/10.1007/S10973-018-7935-Y/TABLES/5.

[11] L.T. Temane, S.S. Ray, J.T. Orasugh, Review on Processing, Flame-Retardant Properties, and Applications of Polyethylene Composites with Graphene-Based Nanomaterials, Macromol Mater Eng 309 (2024) 2400104. https://doi.org/10.1002/MAME.202400104.

[12] B. Anwajler, J. Szołomicki, P. Noszczyk, M. Baryś, The Potential of 3D Printing in Thermal Insulating Composite Materials—Experimental Determination of the Impact of the Geometry on

Thermal Resistance, Materials 2024, Vol. 17, Page 1202 17 (2024) 1202. https://doi.org/10.3390/MA17051202.